JCI insight

RESEARCH ARTICLE

# KCNQ/M-channels regulate mouse vagal bronchopulmonary C-fiber excitability and cough sensitivity

**Hui Sun,[1] An-Hsuan Lin,[2] Fei Ru[1], Mayur J. Patil,[1] Sonya Meeker,[1] Lu-Yuan Lee,[2] and Bradley J. Undem[1]**

[1]Department of Medicine, Johns Hopkins University School of Medicine, Baltimore, Maryland, USA. [2]Department of Physiology, University of Kentucky, Lexington, Kentucky, USA.

**Increased airway vagal sensory C-fiber activity contributes to the symptoms of inflammatory airway diseases. The KCNQ/$K_v$7/M-channel is a well-known determinant of neuronal excitability, yet whether it regulates the activity of vagal bronchopulmonary C-fibers and airway reflex sensitivity remains unknown. Here we addressed this issue using single-cell RT-PCR, patch clamp technique, extracellular recording of single vagal nerve fibers innervating the mouse lungs, and telemetric recording of cough in free-moving mice. Single-cell mRNA analysis and biophysical properties of M-current ($I_M$) suggest that KCNQ3/$K_v$7.3 is the major M-channel subunit in mouse nodose neurons. The M-channel opener retigabine negatively shifted the voltage-dependent activation of $I_M$, leading to membrane hyperpolarization, increased rheobase, and suppression of both evoked and spontaneous action potential (AP) firing in nodose neurons in an M-channel inhibitor XE991–sensitive manner. Retigabine also markedly suppressed the α,β-methylene ATP–induced AP firing in nodose C-fiber terminals innervating the mouse lungs, and coughing evoked by irritant gases in awake mice. In conclusion, KCNQ/M-channels play a role in regulating the excitability of vagal airway C-fibers at both the cell soma and nerve terminals. Drugs that open M-channels in airway sensory afferents may relieve the sufferings associated with pulmonary inflammatory diseases such as chronic coughing.**

## Introduction

The $K_v$7 subfamily of voltage-gated potassium channels, encoded by *KCNQ* genes, exerts critical physiological functions. This is highlighted by the fact that mutations occurring in the 5 members of the *KCNQ* gene family have been found to cause human genetic disorders such as long-QT syndrome with fatal cardiac arrhythmias, epilepsy, encephalopathy, myokymia, deafness, and a congenital neurological disorder with intellectual disability (1, 2). Of the currently identified 5 members of *KCNQ* gene family, *KCNQ2–5*, coding for the pore-forming $K_v$7.2–7.5 α-subunits, are expressed in the nervous system and generate a low-threshold-activated and non-inactivating $K^+$ current, originally termed M-current ($I_M$) when it was identified in the sympathetic neurons as a $K^+$ conductance suppressed by muscarinic receptor activation (3). The KCNQ/$K_v$7 channels underlying the $I_M$, also called M-channels, are ideally suited to control and regulate neuronal membrane potential and excitability because they are constitutively activated at subthreshold potentials and subject to modulation by an array of neurotransmitters and inflammatory mediators signaling through the $G_{q/11}$-coupled receptors (4, 5).

Since the discovery of *KCNQ2/3* mutations associated with human early-onset epilepsies 20 years ago (6–8), the KCNQ/M-channels have been extensively studied in the brain. Compelling evidence has established the KCNQ/M-channel as a potential target for the treatment of a wide range of hyperexcitability-associated neuronal and psychiatric disorders (9, 10) and, particularly, led to the approval of M-channel opener retigabine for clinical use to treat certain forms of epilepsy (11). Functional M-channels have also been found throughout the somatosensory system from afferent terminals to central neurons in spinal cord and thalamus, and increasingly are recognized as playing a role in pain signaling (12–14). Opening M-channels attenuates nociceptive behaviors in various animal models of pain, including inflammatory, neuropathic, and cancer pain (13, 15).

**Conflict of interest:** The authors have declared that no conflict of interest exists.



**Submitted:** August 24, 2018
**Accepted:** January 29, 2019
**Published:** March 7, 2019

**Reference information:**
*JCI Insight*. 2019;4(5):e124467.
https://doi.org/10.1172/jci.insight.124467.

By contrast, whether KCNQ/M-channels contribute to the regulation of airway sensory afferent excitability has not been explored. In fact, studies of M-channels in the visceral sensory system have been sparse and limited to the modulation of aorta baroreceptor activities (16) and nociception in gut tissues (17, 18). Airway sensory afferent nerves, mainly derived from neurons in the vagal sensory ganglia, are critical in initiating reflex responses to harmful stimuli to protect airways and fine-tune cardiopulmonary functions. The majority of vagal sensory afferents terminating in the respiratory tract are C-fibers that are characterized by expression of TRPV1. When stimulated, C-fibers mediate urge to cough, dyspnea, as well as parasympathetic reflex mucus secretion and bronchoconstriction. C-fibers can be activated by mediators of inflammation, contributing to negative symptoms in inflammatory airway diseases (reflex bronchospasm, secretions, and nonproductive coughing) (19). Therefore, ion channels that control the excitability of airway vagal C-fibers may be an attractive therapeutic target aimed at reducing the symptoms of those with inflammatory airway diseases. In this study, we address the hypotheses that M-channels play a role in regulating the excitability of vagal C-fibers in mouse lungs, and that opening the M-channel inhibits C-fiber–mediated coughing. We characterized the expression of KCNQ genes in airway-specific mouse nodose neurons, critically evaluated $I_M$ in nodose neurons, determined the role of M-channels in regulating the excitability of nodose neurons and C-fiber terminals innervating the lungs, and assessed the effects of M-channel opener retigabine on cough induced by irritant gases in freely moving mice.

## Results

*KCNQ gene expression in mouse nodose neurons and lung-specific nodose neurons*. We first examined KCNQ gene expression in mouse nodose ganglia and found that *Kcnq2–5*, but not *Kcnq1* (using mouse heart as positive control) were consistently expressed. We then further characterized the *Kcnq2–5* expression profile at the single-neuron level to gain insight into the possible subunit compositions of M-channels in mouse nodose neurons. *P2rx2* transcript was used as the marker of nodose neurons (vs. jugular neurons) and *Trpv1* as the marker for capsaicin-sensitive C-fibers (20). We evaluated nodose neurons in general as well as nodose neurons retrogradely labeled by dye injection into the lungs. The *Kcnq* expression patterns were not substantially different between the general population of nodose neurons and lung-specific nodose neurons. As shown in Figure 1, expression of *Kcnq3* mRNA was most prevalent in both unlabeled (24 of 30 cells) and lung-specific (22 of 30 cells) mouse nodose neurons, and in both *Trpv1*-positive and *Trpv1*-negative groups. *Kcnq2* mRNA was detected in about half of neurons, with slightly higher incidence being observed in *Trpv1*-negative groups of both unlabeled (60% vs. 40%) and lung-specific (53% vs. 31%) nodose neurons. About 10% of neurons in both labeled and unlabeled groups expressed *Kcnq5*, mostly in *Trpv1*-positive neurons. *Kcnq4* transcript was rarely detected. It is interesting to note that about 50% of *Trpv1*-positive nodose neurons solely expressed *Kcnq3,* whereas the majority of *Trpv1*-negative neurons coexpressed *Kcnq3* and *Kcnq2*. Only 1–2 *Trpv1*-negative neurons expressed *Kcnq3* alone.

*Characterization of $I_M$ in mouse nodose neurons*. Because of the very similar *Kcnq* expression profiles in unlabeled and lung-specific mouse nodose neurons, we performed patch clamp recordings in unlabeled nodose neurons. The voltage-clamp protocol shown in Figure 2A and M-channel blocker XE991 were used to isolate $I_M$. Representative recordings obtained from one nodose neuron before and during bath application of XE991 and after washout of the drug are shown in Figure 2A (upper panels). XE991 (10 μM) markedly reduced the holding current at –30 mV, abolished the currents elicited by hyperpolarizing steps, partially inhibited the currents induced by depolarization to ≥–15 mV, significantly attenuated the tail currents recorded at –60 mV ($I_{tail}$), and completely blocked the slowly activating current elicited by stepping back to holding potential ($V_h$ ) from –60 mV. Upon washout of XE991, the inhibition of currents observed at voltages ≥–5 mV was largely relieved. However, the inhibitory effects of XE991 on currents recorded at voltages negative to –15 mV (including the currents reactivated by steps from –60 mV to $V_h$) and the corresponding $I_{tail}$ could not be reversed by washout of the drug, suggesting that these currents are mediated by M-channels, which have been showed to be irreversibly blocked by XE991 (21, 22). These effects are well illustrated with total XE991-sensitive currents, obtained by digital subtraction of currents recorded in the presence of XE991 from those recorded under control conditions; reversible XE991-sensitive currents, obtained by digital subtraction of currents recorded in the presence of XE991 from those recorded after washout of the drug; and irreversible XE991-sensitive currents, derived by digital subtraction of currents recorded after washout of XE991 from those under the control condition (Figure 2A, lower panels). The latter is smaller

in amplitude and mainly a non-inactivating current component that appears to reach its maximum around –15 mV, then decreases at more positive potentials (for the sake of clarity, only current traces recorded up to –5 mV are shown). By contrast, the currents reversibly blocked by XE991, believed to be mediated by $K_v2.1$ channels (21), activated at more positive voltages, had different kinetics, and were associated with a smaller and faster $I_{tail}$.

We further characterized the sustained component of irreversible XE991-sensitive currents. The apparent reversal potential ($E_{rev}$) was determined by examining the current-voltage (I-V) relationships of instantaneous ($I_{in}$) and sustained currents ($I_{ss}$) induced by hyperpolarizing steps from $V_h$ to –85 through –35 mV during the first voltage pulse (Figure 2B). The intersection of two I-V curves gave an estimate of $E_{rev}$, which was found to be –81.4 ± 0.7 mV ($n$ = 9), similar to the calculated equilibrium potential for $K^+$ ($E_K$, –83.2 mV) based on the $K^+$ concentrations in bath and pipette solutions.

The deactivation of irreversible XE991-sensitive currents elicited by hyperpolarization from $V_h$ to –75 through –45 mV was best fitted by a biexponential function. The mean fast ($\tau_{fast}$) and slow time constants ($\tau_{slow}$) obtained from 5 cells where the current was large enough for accurate curve fitting are plotted against the voltage in Figure 2C. Both $\tau_{fast}$ and $\tau_{slow}$ tended to be faster at more negative voltages between –45 and –65 mV ($P$ = 0.06, 2-way ANOVA). The activation of the current induced by stepping back to $V_h$ following a full deactivation at –60 mV was best fitted to a monoexponential function with a time constant of 205 ± 34 ms ($n$ = 9).

The voltage-dependent activation properties of XE991-sensitive currents were determined by analyzing $I_{tail}$, whose amplitude reflects the fraction of channels opened at the end of prior voltage steps ($V_m$). The amplitude of total, reversible, and irreversible XE991-sensitive $I_{tail}$ obtained from the cell shown in Figure 2A is plotted against $V_m$ in the left panel of Figure 2D. Total and irreversible XE991-sensitive currents both activated around –65 mV and followed the same trajectory up to –25 mV. The irreversible component reached a plateau at –15 mV, 10 mV negative to the total XE991-sensitive $I_{tail}$. The reversible component activated around –15 mV and contributed substantially to the XE991-sensitive $I_{tail}$ at potentials ≥–5 mV. Eight of 9 neurons studied exhibited a reversible XE991-sensitive component. In 4 of 8 cells, the irreversible XE991-sensitive $I_{tail}$ dominated over the entire examined voltage range, as in the one shown in Figure 2D (left). In the other 4 cells, the reversible, non-$I_M$ component was much larger at positive voltages, as in the example in the right panel of Figure 2D. In both cases, however, the activation of irreversible XE991-sensitive currents declined after reaching the maximum. This inward rectification at more positive potentials was observed in 8 of 9 neurons. The response to capsaicin was tested in 7 of 9 neurons. The degree of inward rectification, measured as the percentage of current decline at +25 mV, appeared to be greater in capsaicin-responsive neurons (4 of 7; 42.6% ± 10.9%) compared with neurons insensitive to capsaicin (3 of 7; 22.2% ± 6.2%). Finally, fitting the I-V curves of the irreversible XE991-sensitive $I_{tail}$ to Boltzmann function gave rise to a maximal conductance ($G_{max}$) of 6.5 ± 1.8 nS/pF, with $V_{0.5}$ at –38.2 ± 2.9 mV and a slope factor of 7.6 ± 1.0 mV ($n$ = 9). The mean normalized activation curve is shown in Figure 2E (filled circles and solid curve).

Thus, the sustained component of irreversible XE991-sensitive currents recorded in mouse nodose neurons not only exhibited the major biophysical properties characterizing $I_M$ (5, 23) — such as substantial activation in subthreshold voltage range, being reversed at $E_K$, low current density, slow deactivation and activation rates, and lack of inactivation — but also displayed pronounced inward rectification at positive voltages. Furthermore, detailed analyses of $I_{tail}$ recordings revealed that the sustained current sensitive to XE991 was essentially $I_M$ in the voltage range from channel activation threshold to maximal activation potential (–15 mV) under our experimental conditions; to characterize the voltage-dependent activation of $I_M$ over a broader voltage range, however, obtaining the current irreversibly blocked by XE991 is necessary.

We also evaluated the XE991-sensitive current at a more physiological holding potential (–70 mV) in the absence of any other channel blockers. This experimental setting not only facilitated the recording of both $I_M$ and action potentials (APs) on the same cell, but also helped detect off-target effects of XE991 on other channels, which was important for interpreting correctly the effects of M-channel inhibition by this agent on AP firing in both nodose neurons and terminals. The XE991-sensitive currents were obtained on 8 neurons using the same voltage-clamp protocol as that shown on Figure2A, except that $V_h$ was set at –70 mV. The non-inactivating XE991-sensitive current reached its maximum at –15 mV, so was the associated $I_{tail}$ recorded upon repolarization to –60 mV (data not shown). The activation parameters $G_{max}$ (10.2 ± 1.3 nS/pF), $V_{0.5}$ (–38.3 ± 2.1 mV), and k value (7.0 ± 0.5 mV) obtained in cells held at –70 mV were not statistically different from those derived from $I_M$, defined as the irreversible XE991-sensitive currents recorded

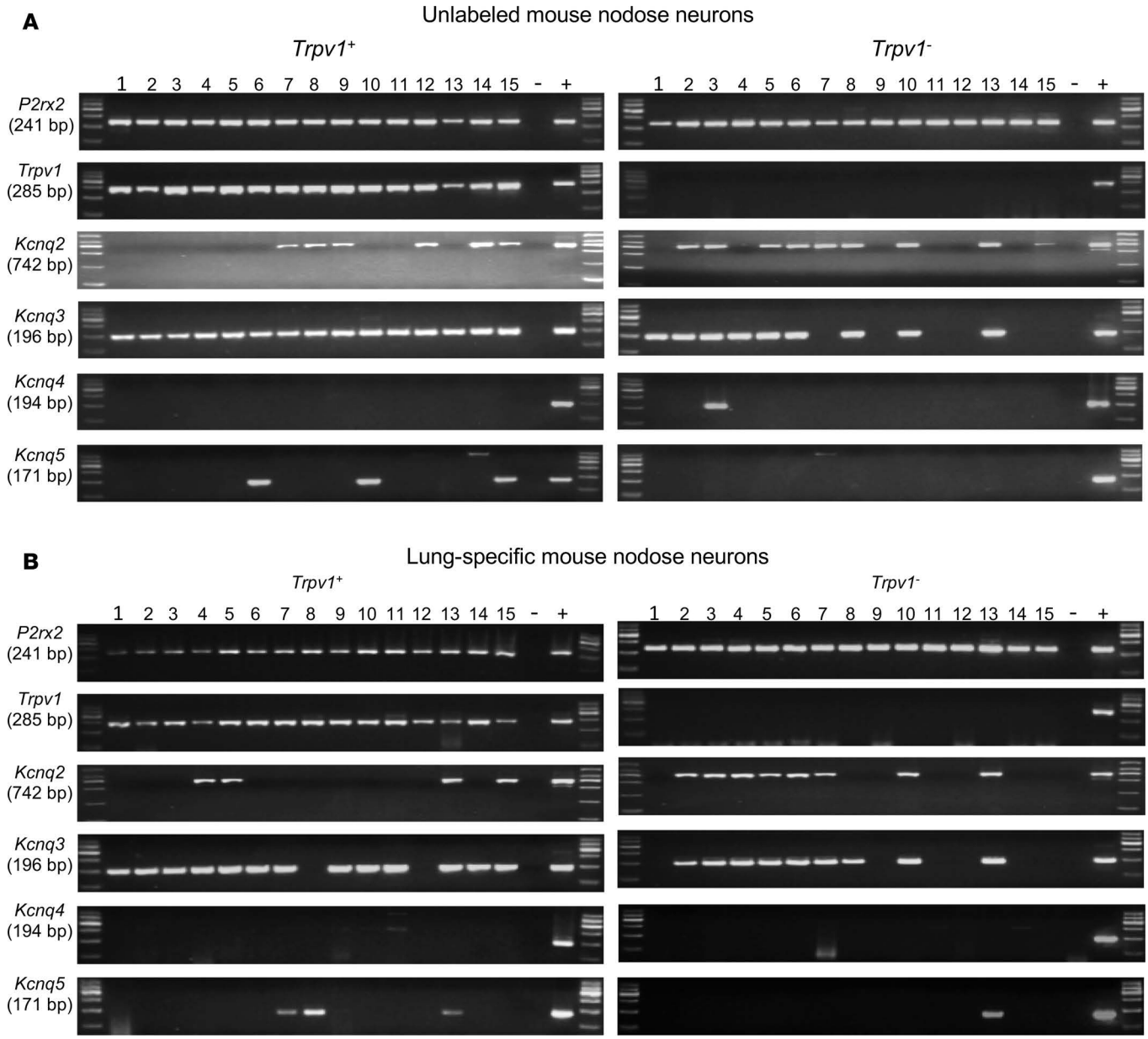


**Figure 1. Expression profile of *Kcnq* transcripts in nodose neurons.** (**A**) Unlabeled mouse nodose neurons. (**B**) Lung-specific mouse nodose neurons. Each lane (numbered on the top of gel images) shows results obtained from one neuron. –, negative control; +, positive control. Mid-range DNA ladder was used for *Kcnq2* amplicon, and the bands read 2000, 1000, 750, 500, 250, and 100 bp from the top. 100-bp ladder was used for amplicons of other genes, and the bands read 600 to 100 bp from the top, with 100-bp decrement. The size of amplicons is given below the gene name.

with the $V_h$ of –30 mV ($P = 0.13$, $P = 0.44$, and $P = 0.16$, respectively). The mean normalized activation curves obtained with $V_h$ at –70 mV and –30 mV were almost superimposable (Figure 2E), confirming that $I_M$ was the major sustained current blocked by XE991 at subthreshold voltages in nodose neurons held at the physiological potential. While holding the neurons at –70 mV, we also noticed that XE991 (10 μM) reduced a fast inward current activated around –45 mV.

*Effects of M-channel opener retigabine on $I_M$ in mouse nodose neurons.* Figure 3A shows representative current traces recorded before and after bath application of 10 μM retigabine, and after subsequent addition of 10 μM XE991 in the presence of retigabine. The current traces recorded in the presence of both retigabine and XE991 and in the presence of XE991 alone (after washout of retigabine; data not shown for clarity) were not different, indicating that the effects of retigabine on membrane current are mediated by its action on M-channels. The XE991-sensitive currents, defined as $I_M$, in the absence and presence of retigabine, were derived

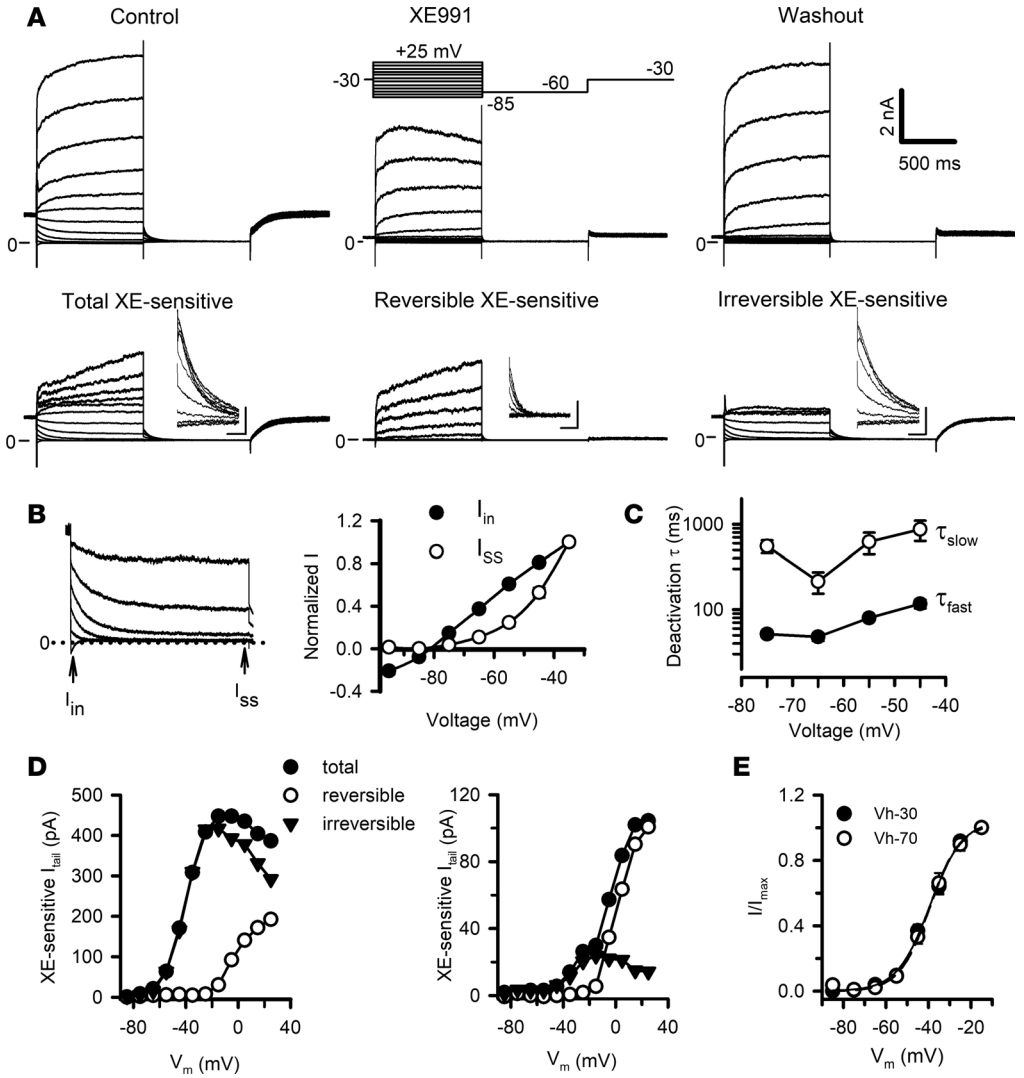


**Figure 2. Characterization of $I_M$ in mouse nodose neurons.** (**A**) Representative current recordings obtained from one of 9 neurons in the absence and presence of 10 μM XE991, and after washout of the drug (upper row) using the voltage clamp protocol shown in the inset; and XE991-sensitive currents obtained by digital subtraction (lower row, see main text). Tail currents ($I_{tail}$) in the lower panels are shown at expanded scale in the inset. Calibration bars: 100 pA and 50 ms. (**B**) Left: The irreversible XE991-sensitive currents evoked by hyperpolarization from $V_h$ to –85 through –35 mV are re-plotted from **A** to illustrate how the instantaneous ($I_{in}$) and sustained currents ($I_{ss}$) were measured. Right: Mean normalized I-V curves of $I_{in}$ and $I_{ss}$ ($n$ = 9). (**C**) Semi-logarithmic plot of deactivation time constants (τ) of irreversible XE991-sensitive currents recorded during the first voltage clamp pulses against voltages ($n$ = 5). (**D**) Amplitudes of total, reversible, and irreversible XE991-sensitive $I_{tail}$ obtained from the neuron shown in **A** (left) and from another neuron (right), respectively, are plotted against the voltages of prior voltage steps ($V_m$). (**E**) Mean normalized activation curves for the irreversible XE991-sensitive current obtained with the $V_h$ at –30 mV ($n$ = 9) and for the XE991-sensitive current recorded with the $V_h$ at –70 mV ($n$ = 8). The solid and dashed curves represent the fit of data points to the Boltzmann function.

by digital subtractions (Figure 3A, lower panel). Retigabine significantly increased the amplitude of $I_M$ tail currents (mean $I_{in}$ amplitude: 195 ±5 1 vs. 146 ± 41 pA, $n$ = 7, $P$ = 0.02) and markedly reduced the current relaxation rate, as indicated by an increased sustained/instantaneous current ($I_{ss}/I_{in}$) ratio (0.74 ± 0.06 vs. 0.11 ± 0.03, $P$ < 0.001). Retigabine also increased the amplitude of sustained current at –30 mV and accelerated the activation rate of $I_M$ evoked by depolarization from –60 to –30 mV (mean activation τ: 149 ± 26 ms vs. 227 ± 50 ms, $P$ = 0.04). The effects of retigabine were readily reversible upon washout (data not shown).

The mean activation curves of $I_M$ obtained in the absence and presence of retigabine are presented in Figure 3B. Retigabine caused a prominent hyperpolarizing shift of $I_M$ activation ($V_{0.5}$ from –39.2 ± 3.5 mV to –71.0 ± 1.4 mV, $P$ < 0.05, Wilcoxon's signed-rank test) without significant effects on $G_{max}$ (7.7 ± 2.7 at

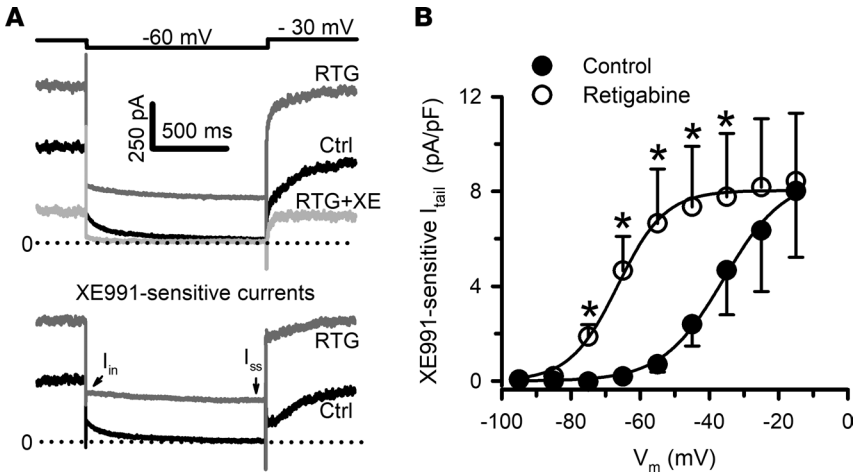


**Figure 3. Effects of retigabine on $I_M$ in mouse nodose neurons.** (**A**) Representative current recordings obtained from one of 7 mouse nodose neurons under the control condition (Ctrl), in the presence of 10 μM retigabine (RTG), and after subsequent addition of 10 μM XE991 in the presence of retigabine (RTG+XE). $I_M$, as defined by XE991-sensitive currents, in the absence (Ctrl) and presence of retigabine, was derived from the original recordings shown in the upper panel by digital subtraction of the current recorded in the presence of XE991 from that obtained under the control condition, and by digital subtraction of the current recorded in the presence of both retigabine and XE991 from that recorded in the presence of retigabine alone. Dotted line represents the zero-current level. Where the instantaneous ($I_{in}$) and sustained ($I_{SS}$) tail currents were measured is indicated. (**B**) Mean activation curves obtained from XE991-sensitive tail currents recorded in the absence and presence of 10 μM retigabine ($n$ = 6). *$P$ = 0.015 at –75 mV, 0.024 at –65 mV, 0.037 at –55 mV, 0.031 at –45 mV, and 0.031 at –35 mV by paired $t$ test or Wilcoxon's signed-rank test when normality test failed.

baseline vs. 8.1 ± 2.9 nS/pF with retigabine, $P$ = 0.78) or $k$ values (7.3 ± 0.9 at baseline vs. 9.2 ± 0.5 with retigabine, $P$ = 0.06). Although the maximal conductance of M-channel in mouse nodose neurons was not altered by retigabine, the drug significantly increased the channel opening over voltages from –80 to –30 mV, with more than 50% of channels being open around the resting potential. These results are consistent with previously reported effects of retigabine on $I_M$ in various cell types (10).

*Effects of pharmacologically modulating $I_M$ on resting membrane potentials and spontaneous firing in mouse nodose neurons*. Figure 4 shows typical recordings and pooled data illustrating the effects of retigabine and/or XE991 on the resting potential of mouse nodose neurons. Retigabine (10 μM) hyperpolarized the cells by an average of 12 mV (from –60.8 ± 0.7 to –72.9 ± 0.6 mV, $n$ = 24). This effect was readily reversible upon washing out the drug or by subsequent application of XE991, suggesting that the retigabine-induced hyperpolarization was mediated via its action on M-channels (Figure 4, A and B). Bath application of XE991 caused a small but significant membrane depolarization (Figure 4, C and D), even in the presence of retigabine (Figure 4, A and B). Addition of retigabine in the presence of XE991 caused a transient hyperpolarization (Figure 4C, upper panel), probably due to the opening of originally closed $I_M$ channels that were subsequently blocked by XE991. In support of this idea, a second application of retigabine did not cause apparent changes in membrane potential. Similarly, retigabine applied after the cell was stimulated to fire the AP repetitively for 3–5 minutes in the presence of XE991 did not induce membrane hyperpolarization (Figure 4C, lower panel). The mean value of resting potentials measured at steady state following application of retigabine in the presence of XE991 is shown in Figure 4D. These results further confirm that retigabine causes membrane hyperpolarization by activating available M-channels. These observations are also in agreement with the recent finding that the blocking effects of XE991 on KCNQ channels are state dependent and favor the activated channels (22). Finally, the depolarization caused by XE991 was not reversible, consistent with the irreversible block of $I_M$ by this agent.

Spontaneous AP firing was observed in 3 of more than 60 mouse nodose neurons examined under current clamp in this study. One example is shown in Figure 4E. Bath perfusion of retigabine hyperpolarized the membrane and nearly abolished the spontaneous activity. Addition of XE991 in the presence of retigabine reversed the hyperpolarization followed by a persistent AP discharge. The inhibitory effects of opening M-channels on spontaneous AP firings were also observed in the other 2 neurons.

*Effects of pharmacologically modulating $I_M$ on excitability of nodose neurons*. To determine further the role of $I_M$ in the regulation of nodose neuron excitability, we examined the effects of retigabine and XE991 on rheobase, AP threshold, and AP numbers in response to suprathreshold stimulation. Retigabine increased the rheobase by an average of 4-fold in 14 cells studied (Figure 5, A and B, left). This is consistent with a large reduction of input resistance around the resting potential of the cells induced by retigabine (from 974 ± 12 to 227 ± 58 MΩ, $n = 16$, $P < 0.001$). XE991 significantly increased the input resistance (from 907 ± 15 to 1297 ± 16 MΩ, $n = 11$, $P = 0.02$), but had variable effects on the rheobase: increasing in 8 of 18 cells, decreasing in 4 of 18 cells, and unchanged in 6 of 18 cells, resulting in an unchanged mean value compared with baseline (Figure 5, A and B, middle). Similar effects were observed when retigabine was applied in the presence of XE991 or vice versa (Figure 5, A and B, right). The different effects of XE991 on the rheobase among different cells did not seem to be related to the amplitude of $I_M$ measured on the same cells ($n = 8$, $r = 0.16$) or degree of XE991-induced depolarization ($n = 18$, $r = 0.09$). In contrast to its effect on the rheobase, retigabine did not alter the AP threshold, while XE991, paradoxically, increased it regardless of whether retigabine was present (Figure 5C). Reduced AP amplitude (116 ± 4 vs. 122 ± 3 mV, $n = 20$, $P < 0.001$) and peak of the rate of AP upstroke (147 ± 10 vs. 163 ± 9 V/s, $n = 20$, $P = 0.007$) were also observed in the presence of XE991.

The number of APs evoked by a 1-second depolarizing current in mouse nodose neurons increased when the amount of injected current increased from 2-fold to 5-fold rheobase, without a further increase at 10-fold rheobase (Figure 5D). Retigabine effectively lowered AP numbers in response to stimuli of all 3 intensities, an effect completely reversible upon washout (Figure 5D, left). XE991 did not, however, significantly affect the AP firing evoked by suprathreshold stimulations (Figure 5D, right). We also examined the effect of retigabine and XE991 on AP firing evoked by a suprathreshold stimulation of the same intensity (1 nA for 1 second). Again, the AP number was decreased in the presence of retigabine, but not significantly changed by XE991 (Figure 5E).

*Effects of M-channel modulators on excitability of vagal C-fibers innervating the mouse lungs*. We next examined whether M-channel activities play a role in regulating the excitability of vagal sensory C-fiber terminals in the mouse lung, key sites for initiation of APs. We have previously shown that α,β-methylene–ATP (α,β-MeATP) evokes AP discharge in mouse and guinea pig nodose C-fibers via activation of $P2X_2/P2X_3$ heterotrimeric ion channels (20, 24). In the present study, repetitive applications of 3 μM α,β-MeATP activated mouse nodose C-fibers with similar AP firing (AP numbers: 39 ± 11 and 47 ± 14 for the first and second agonist stimulation, $n = 10$). In fibers pretreated with 10 μM retigabine, however, the agonist failed to evoke any AP in 5 of 7 fibers and induced only 1 or 2 APs in the other 2 fibers (Figure 6B). Retigabine also abolished the spontaneous activity observed in 4 fibers; one example is shown in Figure 6C. Pretreatment of the lungs with 10–30 μM XE991 prevented retigabine from abolishing the α,β-MeATP–induced AP firing (Figure 6D), suggesting that retigabine suppressed mouse lung C-fiber excitability via opening the M-channels at the nerve endings. XE991 per se did not increase the excitability of the C-fiber terminals. In fact, the average number of APs evoked by 3 and 10 μM α,β-MeATP was reduced in the presence of XE991, albeit not in a statistically significant manner (48 ± 24 APs for control vs. 24 ± 7 APs with XE991, $n = 6$, $P = 0.21$; and 45 ± 16 APs for control vs. 31 ± 7 APs with XE991, $n = 6$, $P = 0.19$, respectively).

*Effects of XE991 on sodium current in mouse nodose neurons*. Our results show that XE991 tends to inhibit agonist-evoked AP firing in mouse bronchopulmonary C-fibers, has a variable effect on the rheobase, and paradoxically increases the AP threshold in nodose neurons, accompanied by a reduction in AP amplitude and in the maximal rate of AP upstroke. We also observed that XE991 reduced a fast inward current by about 25% when nodose neurons were held at –70 mV to record $I_M$. These findings prompted us to examine whether XE991 has an off-target effect on $Na^+$ currents ($I_{Na}$), which are critical to AP initiation and conduction, in mouse nodose neurons. We have previously shown that mouse nodose neurons mainly express $Na_V1.7$, $Na_V1.8$, and $Na_V1.9$ (25), and in guinea pig nodose neurons that $Na_V1.7$ mediates the fast tetrodotoxin-sensitive (TTX-sensitive) $I_{Na}$ and $Na_V1.8$ mediates the slower TTX-resistant $I_{Na}$ (26). To evaluate the effects of XE991 on $I_{Na}$, the nodose neurons were held at –120 mV, and 2 depolarizing pulses, separated by a 1-second interval at –70 mV, were applied every 15 seconds to voltages that elicited the maximal $I_{Na}$ (Figure 7A). In 2 of 4 neurons studied with this protocol, a slower $I_{Na}$ component contributed significantly to the total current. Figure 7 presents the results obtained from a neuron that mainly expressed the fast $I_{Na}$ (Figure 7B) and from a neuron that had a substantial slow component of $I_{Na}$ (Figure 7C). Bath application of XE991 significantly reduced the amplitude of total $I_{Na}$ in both cells, with greater effects being found on the currents elicited from –70 mV, a voltage more relevant to physiological conditions. For the neuron shown in Figure

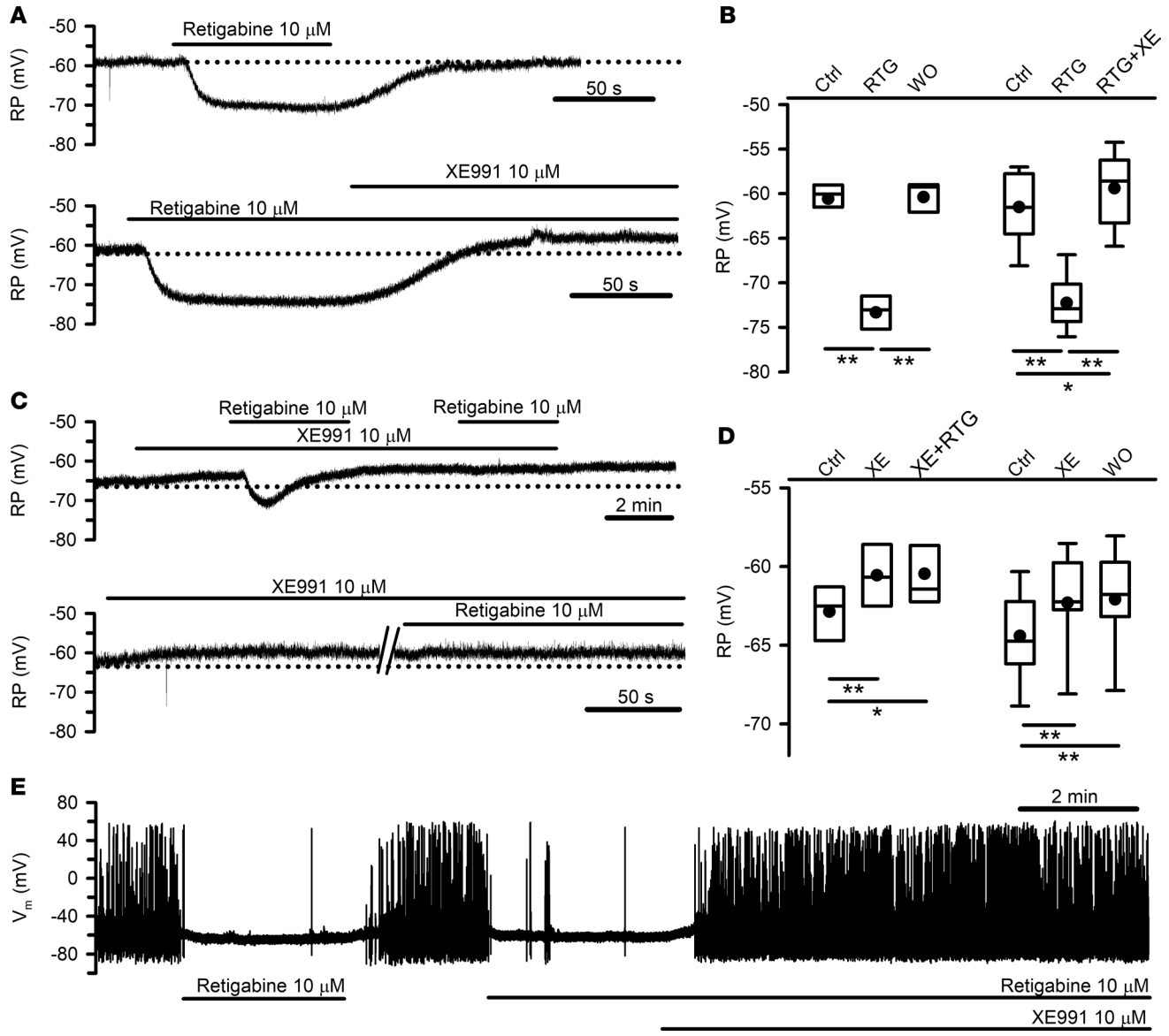


**Figure 4. Effects of retigabine and/or XE991 on resting potentials and spontaneous AP firing in mouse nodose neurons.** (**A**) Representative recordings of membrane potential obtained from 2 different neurons. Bath application of retigabine and XE991 is indicated by the horizontal bars at the top of the recordings. Dotted lines indicate control resting potential (RP) levels. (**B**) Quantification of RP values measured from 2 groups of neurons ($n$ = 6 and 12, respectively) under the control condition (Ctrl), in the presence of retigabine (RTG), and after washout of retigabine (WO), or after subsequent addition of XE991 to retigabine-containing bath solution (RTG+XE) as in the examples shown in **A**. *$P$ = 0.006, **$P$ < 0.001. (**C**) Representative recordings of membrane potential obtained from 2 different neurons. Dotted lines indicate control RP levels. The break symbol in the lower trace represents a 5-minute interval during which the cell was repetitively stimulated to fire the APs with suprathreshold current injections in the constant presence of XE991. (**D**) Quantification of RP values measured from 2 groups of neurons ($n$ = 8 and 10, respectively) at baseline (Ctrl), in the presence of XE991 (XE), and after addition of retigabine in the presence of XE991 (XE+RTG), or after washout of XE991 (WO). *$P$ = 0.004, **$P$ < 0.001. (**E**) Representative recordings of membrane potential showing the effects of retigabine and XE991 on spontaneous AP firing. Box-and-whisker plots in **B** and **D**: Horizontal lines of boxes represent 25th percentile, median, and 75th percentile. Whiskers represent 5th/95th percentile. Filled circles represent mean values. Statistical significance was determined by 1-way repeated-measures ANOVA with Holm-Šídák test as a post hoc analysis.

7C, the fast $I_{Na}$ elicited from –70 mV was largely inhibited by 30 μM XE991, leaving out the slow $I_{Na}$ component. In 3 neurons where the effects of XE991 at both 10 and 30 μM were examined, the total $I_{Na}$ evoked from –120 mV was inhibited by 13% ± 2% and 27% ± 6%, and the current elicited from –70 mV reduced by 31% ± 5% and 53% ± 12% by 10 and 30 μM XE991, respectively. These results reveal a substantial inhibitory effect of XE991 on fast $I_{Na}$ in mouse nodose neurons. Therefore, the effect of this M-channel blocker on neuronal excitability in any given mouse nodose neuron is likely the net effect of opposing actions induced by inhibition of $I_M$ and inhibition of $I_{Na}$.

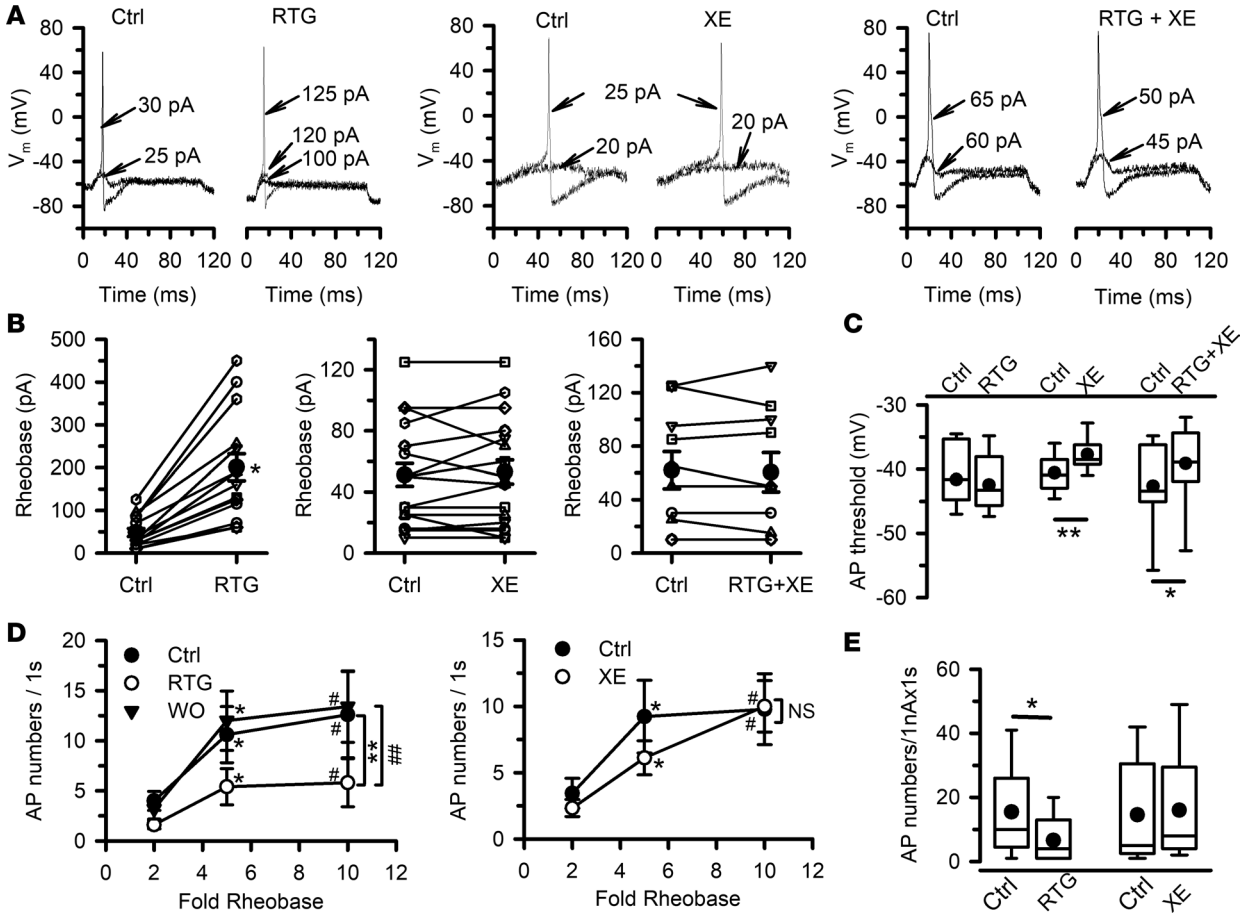


**Figure 5. Effects of retigabine and/or XE991 on excitability of mouse nodose neurons.** (**A**) Representative recordings of membrane potential showing the smallest amount of depolarizing current needed to evoke an AP (rheobase) at baseline (Ctrl) and after application of retigabine (RTG), XE991 (XE), or retigabine in the presence of XE991 (RTG+XE). (**B**) Changes in rheobase by application of retigabine (left, $n = 14$), XE991 (middle, $n = 18$), or retigabine in the presence of XE991 (right, $n = 10$). Open symbols and lines indicate the change for individual cells. Filled circles and error bars represent mean ± SEM of the group. $^{*}P < 0.001$ (paired $t$ test). (**C**) Quantification of AP threshold obtained from 3 groups of neurons before (Ctrl) and after application of retigabine (RTG, $n = 14$), XE991 (XE, $n = 18$), or both retigabine and XE991 (RTG+XE, $n = 10$). $^{*}P = 0.001$. $^{**}P < 0.001$ (paired $t$ test). (**D**) Left: Averaged number of APs evoked by 1-second depolarizing current as a function of the injected current intensity (defined as fold rheobase) obtained from 5 cells in the absence and presence of 10 μM retigabine, and after washout of the drug (WO). $^{*}P = 0.023$, and $^{\#}P = 0.01$ compared with AP numbers at 2-fold rheobase. $^{**}P = 0.008$, $^{\#\#}P = 0.005$ between 2 conditions as indicated. Right: Similar plots of data obtained from 9 cells under the control condition and in the presence of 10 μM XE991. $^{*}P = 0.002$, $^{\#}P < 0.001$ compared with AP numbers at 2-fold rheobase. NS: $P = 0.4$ between 2 groups. Statistical significance was determined by 2-way repeated-measures ANOVA with Holm-Šídák test as a post hoc analysis. (**E**) Quantification of AP numbers in response to the same suprathreshold stimulation (1 nA for 1 second) obtained from 2 groups of neurons before and after treatment with retigabine, and before and after treatment with XE991, respectively. $n = 9$ for both groups. $^{*}P = 0.01$ (paired $t$ test). Box-and-whisker plots in **C** and **E**: Horizontal lines of boxes represent 25th percentile, median, and 75th percentile. Whiskers represent 5th/95th percentile. Filled circles represent the mean values.

*Effects of the M-channel opener retigabine on irritant gas–induced cough in awake mice*. To determine whether activating M-channels at the bronchopulmonary C-fiber terminals inhibits in vivo airway reflex responses, we examined the effects of nebulized retigabine on cough induced by irritant gases in awake mice. Coughs were identified by the 3 distinct but tightly connected phases of the synchronized changes in both chamber pressure ($P_{cham}$) and intrapleural pressure ($P_{ip}$; Figure 8A), generated by the initial inspiratory effort followed by chest compression and a forced expiration. Typically, $P_{ip}$ rose sharply to >40 mmHg at the end of the chest compression. The forced expiration coincided with a detectable cough sound (data not shown). Cough was generally not detected before inhalation challenge (Figure 8, B and C). Both $SO_2$ and $NH_3$ inhalation challenges evoked coughs in a concentration-dependent manner ($P <$ 0.01 between 300 and 600 ppm $SO_2$; and $P < 0.05$ between 0.1% and 0.2% $NH_3$).

Following retigabine inhalation, cough responses to both low and high concentrations of $SO_2$ were almost completely blocked (Figure 8, A–C). The inhibitory effect of retigabine on $NH_3$-evoked coughs was more modest, particularly at the higher concentration of $NH_3$ (43% inhibition, Figure 8, B and C). The antitussive

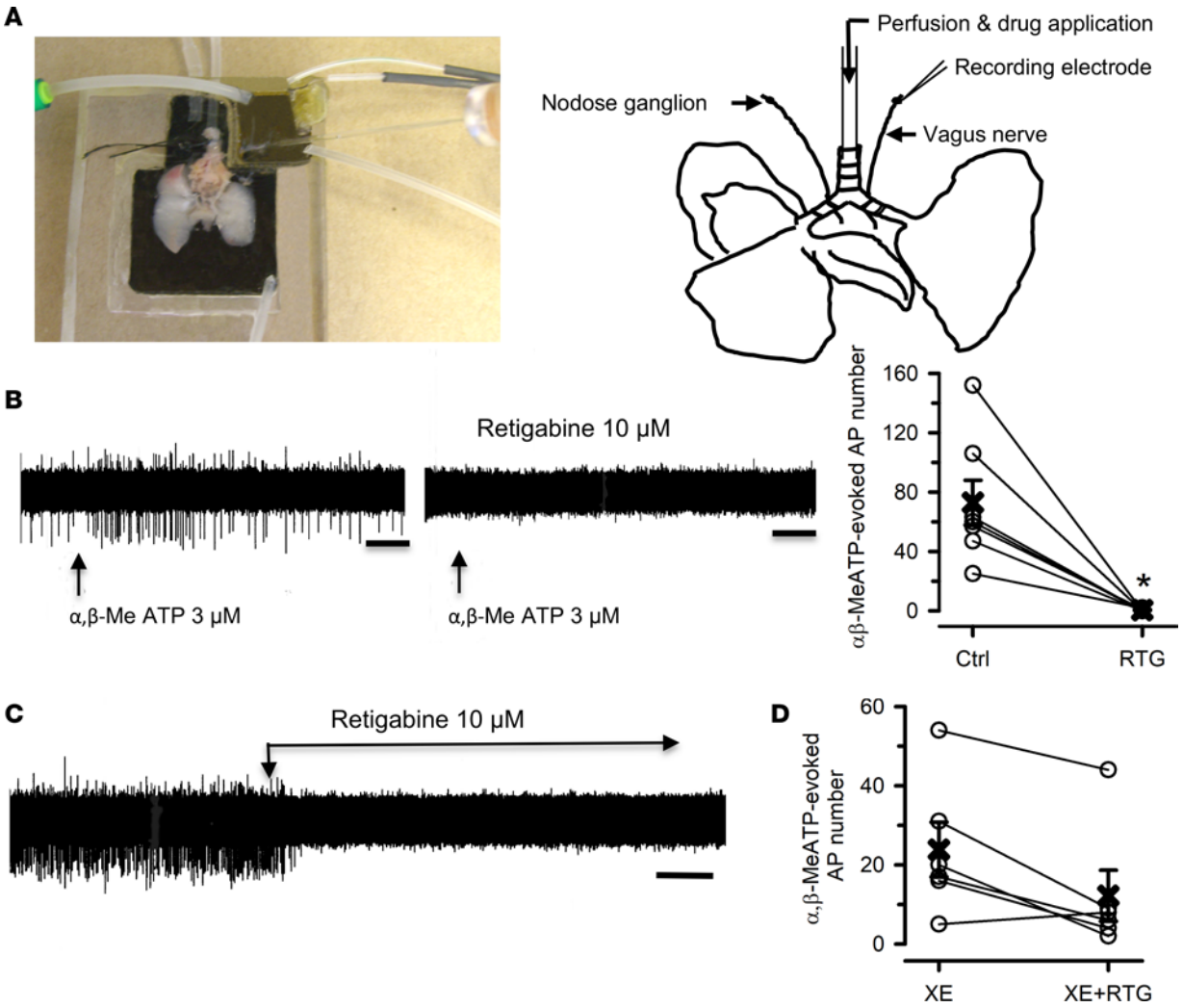


**Figure 6. Effects of M-channel modulators on AP discharge in mouse bronchopulmonary nodose C-fibers.** (**A**) Image (left) and schematic representation (right) of a trachea-perfused mouse lung vagus nerve preparation. (**B**) Representative traces (left) and group data (right, $n = 7$) of α,β-MeATP–induced AP firing recorded from mouse lung nodose C-fibers before (Ctrl) and after treatment with retigabine (RTG; 10 μM for 15 minutes). The fiber shown on the left responded to α,β-Me ATP with a peak firing frequency of 4 Hz. Calibration bar: 10 seconds. In the right panel, open symbols and lines indicate the change in AP number for individual fibers. Bold X and error bars represent mean ± SEM of the group. *$P = 0.004$ (paired $t$ test). (**C**) Recording from one of 4 C-fibers exhibiting spontaneous AP firing (<1 Hz) that was silenced by application of retigabine. Calibration bar: 2 minutes. (**D**) AP numbers in response to 3 μM α,β-MeATP obtained from 6 fibers in the presence of XE991 (XE; 30 μM) and XE991 (30 μM) plus retigabine (10 μM) for 15 minutes. The preparations were perfused with normal Krebs solution for 30 minutes between treatments. Open symbols and lines indicate the changes for individual fibers. Bold X and error bars represent mean ± SEM. Note: AP number in XE991 is less than control (48 ± 24 APs for this group of fibers), which may be due to the inhibition of $I_{Na}$, as discussed in the main text. $P > 0.05$ by 1-way repeated-measures ANOVA.

effect of retigabine was reproducible, as evidenced by similar effects observed when tested on a different day (Figure 8C). The cough responses to irritant gases were fully recovered 24 hours after retigabine treatment, indicating absence of desensitization of responses to irritant gases. Furthermore, vehicle of retigabine (isotonic saline) delivered in the same manner did not have any effect on coughs in 2 mice tested (data not shown).

## Discussion

This study provided the first evidence to our knowledge that M-channel activities regulate the excitability of airway vagal afferent C-fibers and evoked cough responses in mice. The main findings include the following: (i) *Kcnq3* is the most prevalent *Kcnq* transcript found in mouse nodose neurons and in lung-specific nodose neurons, and may form functional homotetrameric channels in these cells; (ii) $I_M$ contributes to maintaining negative resting potential in mouse nodose neurons; (iii) activation of $I_M$ by retigabine suppresses the excitability of mouse nodose neurons via membrane hyperpolarization and reduced input resis-

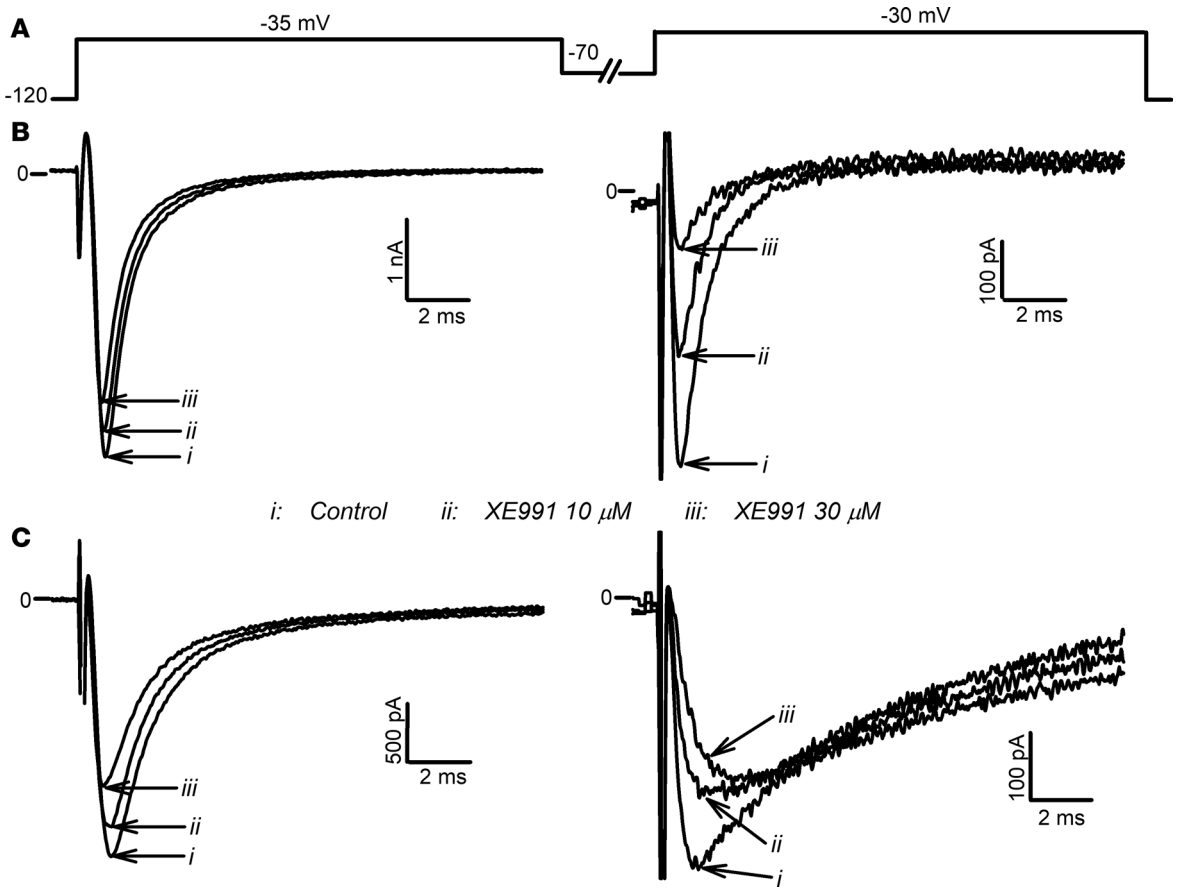


**Figure 7. Effects of XE991 on $Na^+$ currents in mouse nodose neurons.** (**A**) Voltage-clamp protocol consisting of 2 depolarizing pulses to voltages at which the $I_{Na}$ peaks, separated by a 1-second interval at –70 mV ($V_h$, –120 mV). (**B** and **C**) Current recordings elicited by the first (left panels) and the second (right panels) depolarizing step from 2 different nodose neurons under the control condition (i) and after bath application of 10 (ii) and 30 μM (ii) XE991. Note the different scales of the *y* axis among the 4 panels. Similar effects were observed in 4 neurons.

tance; and (iv) nodose C-fiber terminals innervating the mouse lung express functional M-channels, and pharmacologically activating these channels represents a powerful means to inhibit both spontaneous and agonist-evoked AP discharge and to suppress the irritant gas–induced coughing in freely moving mice.

*Characterization of M-channels in mouse nodose neurons*. The $I_M$ in neonatal rat nodose neurons and in baroreceptor neurons of adult rat nodose ganglia has previously been described (16, 21). In this study, we found that $I_M$ in mouse nodose neurons differs from rat nodose $I_M$ in several aspects: (i) mouse nodose $I_M$ displays a higher voltage sensitivity, has a more negative $V_{1/2}$ (–39 vs. –24 mV) and reaches maximal activation at more negative potentials (–15 vs. 0 mV); (ii) it exhibits an inward rectification at positive potentials, which is absent in rat nodose $I_M$; and (iii) the same concentration of retigabine produces a larger hyperpolarizing shift of mouse $I_M$ activation curve ($V_{1/2}$ shifted by –32 mV compared with ≤15-mV left shift of I-V curves in rats ). The different *KCNQ*/$K_V$7 expression profiles in rat and mouse nodose neurons likely contribute to this phenotypic difference. It has been reported that positive immunoreactivities for KCNQ2/$K_v$7.2, KCNQ3/$K_v$7.3, and KCNQ5/$K_v$7.5 subunits were detected in all neonatal rat nodose neurons and in baroreceptor terminals of adult rats (16, 21). In mouse nodose neurons (including lung-specific nodose neurons), however, expression of *Kcnq3* was most prevalent, followed by *Kcnq2*, with and few neurons expressing *Kcnq5*. Notably, 50% of mouse *Trpv1*-positive C-fiber neurons solely expressed *Kcnq3*, and about half of mouse nodose neurons expressed *Kcnq2* along with *Kcnq3*, as most frequently seen in *Trpv1*-negative neurons. Heterologous expression studies have shown that the neuronal KCNQ2–5/$K_v$7.2–7.5 subunits can form functional homomeric M-channels (27–29), whereas coexpression of KCNQ3 with KCNQ2, KCNQ4, or KCNQ5 subunits usually leads to the formation of heterotetrameric channels that generate larger $I_M$ (6, 27, 30). These various homomeric and heteromeric KCNQ/M-channels have distinct biophysical and pharmacological properties. For example, the pronounced inward rectification at positive poten-

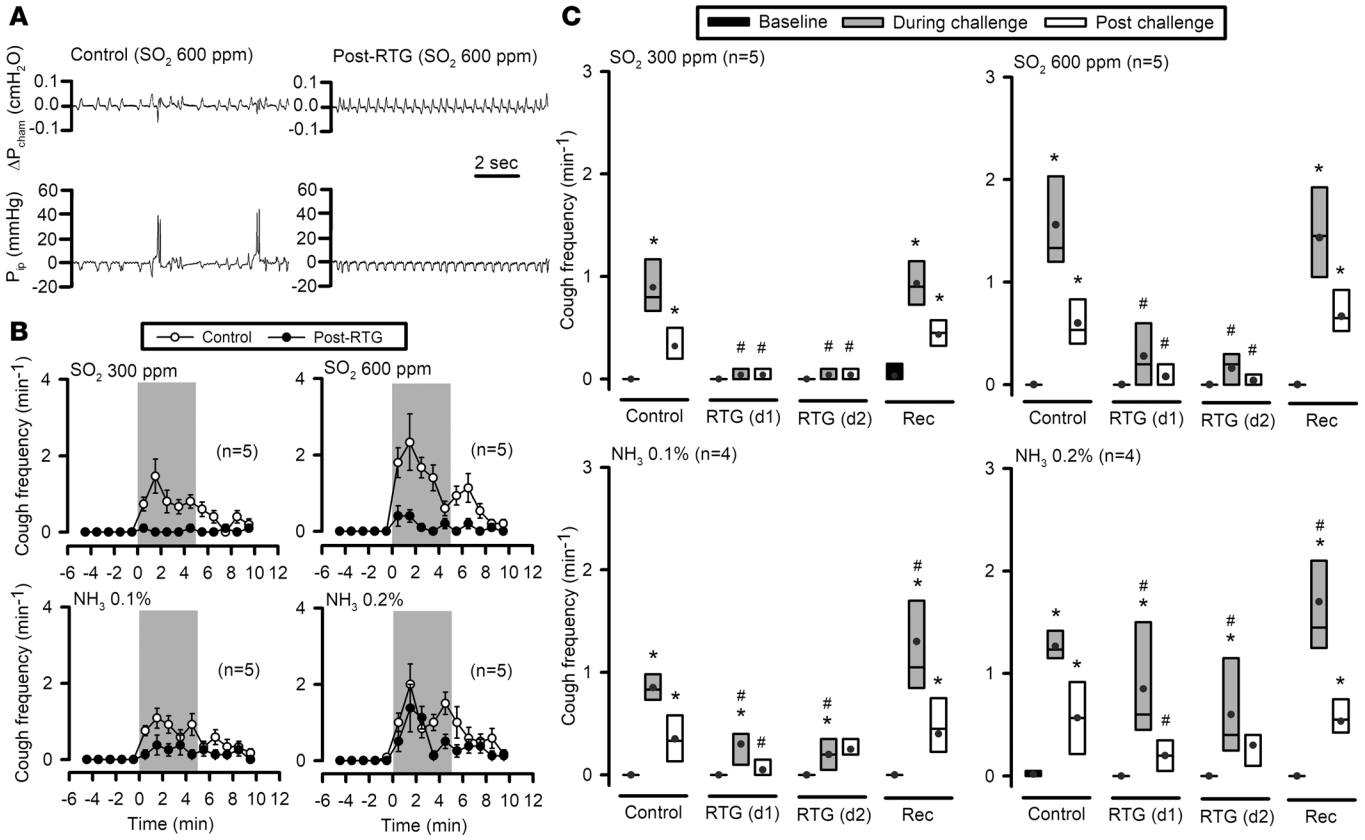


**Figure 8. Effects of retigabine on irritant gas–induced coughing in awake mice.** (**A**) Representative recordings illustrating the effect of nebulized retigabine (RTG) on the cough response to $SO_2$ inhalation challenge. Note the synchronized changes in both recording chamber pressure ($P_{cham}$) and intrapleural pressure ($P_{ip}$) (**B**) Cough frequency in responses to $SO_2$ or $NH_3$ inhalation challenges (marked by the shaded area) under control conditions and post-RTG treatment. (**C**) Box plots of cough frequency at baseline and during and afters $SO_2$ or $NH_3$ challenge (each from a 5-minute recording) before RTG inhalation (Control), after RTG inhalation (tested 2 times on 2 different days: day 1 and d2), and at least 1 day after the last RTG inhalation (Rec, recovery).Horizontal lines of boxes represent 25th percentile, median, and 75th percentile. Filled circles represent mean values. $^*P < 0.05$ vs. baseline; $^\#P < 0.05$ vs. control 2-way repeated-measures ANOVA with Fisher's test as a post hoc analysis for multiple pairwise comparisons. Control data in **B** and **C** were averaged from 3 experiments performed on 3 separate days for each mouse, and post-RTG data in **B** were averaged from 2 experiments on 2 separate days for each mouse.

tials, believed to result from channel inactivation at strong depolarization (28), has been shown to be a characteristic of KCNQ3 or KCNQ5 homomer–mediated whole-cell currents (27–29, 31). Comparative studies on voltage-dependent activation have shown that heterologously expressed KCNQ3/$K_V$7.3 homomers have a more negative $V_{0.5}$ (–29 to –40 mV) and maximal activation voltages (–30 to –10 mV), as well as a steeper slope (5–6 mV vs. ≥10 mV) than KCNQ2, KCNQ4, KCNQ5 homomeric, and KCNQ2/3 heteromeric channels (29, 32–35). Different KCNQ channels also exhibit different sensitivities to retigabine. The same concentration of retigabine (10 μM) caused the largest hyperpolarizing shift of voltage-dependent activation in KCNQ3 homomeric channels, followed by KCNQ2/KCNQ3 and KCNQ3/KCNQ5 heteromeric channels, and then by KCNQ2 and KCNQ4 homomeric channels expressed in CHO cells (33, 36). The $V_{0.5}$ values in the presence of retigabine found in our mouse nodose neurons (–71 mV) and KCNQ3 homomer–expressing cells (–72 mV) (33) are strikingly similar. Although the degree of retigabine-induced negative shift of $I_M$ activation curve observed in this study (by –32 mV) is less than the –43 mV obtained for KCNQ3 channels in CHO cells, it is significantly larger than those found in other native cells, such as large myelinated fibers of rat sciatic nerve (by –24 mV), where nodal $I_M$ is mediated by KCNQ2 homomers (37); as well as neocortical myelinated axons (by –29 mV) (38) and rat sympathetic neurons (by –21 mV) (33), where $I_M$ is mainly mediated by KCNQ2/3 heteromers. Thus, the electrophysiological characteristics of $I_M$ combined with the unique expression profile of *Kcnq* transcripts found in mouse nodose neurons suggest a contribution of KCNQ3 homotetramers to the functional M-channels in a subset of neurons. This is particularly true in *Trpv1*-positive nodose neurons, where *Kcnq3* was the only *Kcnq* subtype expressed in about 50% of the neurons. This inference will remain tentative until additional gene deletion studies are carried out

or until more subtype-selective inhibitors are developed. On the other hand, *Kcnq2* along with *Kcnq3* was expressed in ~30% of *Trpv1*-positive neurons, and in the vast majority of *Trpv1*-negative nodose neurons, consistent with the well-established colocalization of KCNQ2 and KCNQ3 subunits at the nodes of Ranvier in both central and peripheral myelinated fibers (38–40). This expression pattern is also in accordance with the less-inward rectification of $I_M$ at positive potentials observed in capsaicin-insensitive compared with capsaicin-sensitive nodose neurons.

Our finding that KCNQ3/$K_V$7.3 subunits may form functional homomeric M-channels in mouse nodose neurons seems to be at odds with the general impression that KCNQ3/$K_v$7.3 homomers do not generate significant currents. Indeed, a few studies have found no detectable $I_M$ in oocytes expressing rat KCNQ3 (41) or CHO cells expressing human KCNQ3 (42, 43). Many other studies have, however, reported substantial $I_M$ when KCNQ3 was expressed in both oocytes (6, 31) and mammalian cell lines (29, 33–35, 44, 45). In fact, KCNQ3/$K_v$7.3 expressed very well in mammalian expression systems, particularly in tsA cells, such that reliable studies on TEA- (44) or muscarinic receptor activation–induced (29, 45) inhibition of KCNQ3 currents could be performed. Furthermore, it has been shown that KCNQ3 can traffic to the plasma membrane and target to the key sites (nodes of Ranvier and axon initial segment) of neurons, although co-assembly with KCNQ2 increases surface expression of both subunits (46–48). Robust expression of KCNQ3 subunits in nodes of KCNQ2-null sensory neurons has also been reported (39). Therefore, our findings in mouse nodose neurons are not inconsistent with most previously published studies on KCNQ3 channels. Moreover, our study may suggest that these channels likely function better in the native environments.

In addition to the two most prevalent compositions of KCNQ transcripts, *Kcnq3* and *Kcnq3* with *Kcnq2*, expressed in mouse nodose neurons and lung-specific neurons, *Kcnq5* or *Kcnq4* was detected along with *Kcnq2* and/or *Kcnq3* in about 10% of the neurons. Whether the cells expressing different composition of KCNQ genes represent functionally distinct subsets of neurons needs further investigation. In this regard, previous studies have revealed that $K_v$7.4 is expressed in ~10% of mouse DRG neurons and their peripheral projections representing a subset of rapidly adapting, low-threshold mechanoreceptors, and plays a role in modulating touch sensitivity (49); whereas $K_v$7.2 and $K_v$7.3, but not $K_v$7.4 or $K_v$7.5, subunits are expressed in a subset of DRG neurons corresponding to down-hair (D-hair) Aδ low-threshold mechanoreceptors and modulate the mechanosensitivity of D-hairs at their peripheral nerve endings in the skin (50).

*M-channel activities regulate mouse nodose neuron and airway C-fiber excitability, as well as cough response*. Our study showed that $I_M$ started to activate at around –65 mV in mouse nodose neurons and reached about 5% of maximal activation at cells' resting potentials. Hence, inhibition of M-channels by XE991 consistently evoked a small but significant depolarization, indicating that $I_M$ contributes to setting the resting potential in mouse nodose neurons. Opening M-channel by retigabine caused hyperpolarization of an average of 12-mV and profoundly decreased excitability in mouse nodose neurons, as evidenced by a more than 4-fold increase in the rheobase; a markedly reduction in evoked AP numbers; and an abolition of spontaneous AP firing. Our results also showed that retigabine reduced the input resistance at resting potentials without altering the AP threshold, suggesting that membrane hyperpolarization and reduced input resistance are the major mechanisms underlying the effects of retigabine in our cells. In accordance with the findings in the cell soma, applying retigabine to the receptive field of nodose C-fibers in the mouse lungs strongly reduced the agonist-evoked AP discharge and abolished the spontaneous activities. These effects were prevented by pretreatment with XE991, indicating that functional KCNQ/$K_v$7/M-channels are present in nodose C-fiber terminals, where their activation effectively suppresses AP generation.

Although XE991 completely reversed or prevented the inhibitory effects of retigabine on AP discharge in both mouse nodose neurons and C-fiber terminals, an excitatory effect of XE991 per se was not observed. In fact, we found that XE991 caused a slight increase in AP threshold and had a tendency to reduce AP discharge at nodose C-fiber terminals in the lungs. These observations are at odds with the repetitive AP firing induced by focal puff application of XE991 in rat lumbar DRG neurons (51) and with the finding that XE991 modestly increased afferent firing in response to noxious bowel distension in mouse distal colons (17). However, the absence of effects on AP firing properties in mouse sympathetic neurons (52) and an increase in the pressure threshold for rat baroreceptor discharge (16) by XE991 have also been reported. Furthermore, recordings in a skin–saphenous nerve preparation have revealed variable effects of XE991 (53, 54). Our finding that XE991 significantly inhibited the fast $I_{Na}$ in mouse nodose neurons has not to our knowledge been previously reported and may be relevant to this discussion. We previously demonstrated that inhibition of the fast $I_{Na}$, even in neurons that expressed a large slow TTX-resistant $I_{Na}$, substantially increased the amount of

current needed to evoke an AP in guinea-pig nodose and jugular neurons (26). Therefore, the possible excitatory effect of blocking $I_M$ by XE991 in our mouse nodose neurons and terminals may have been offset by XE991-induced $I_{Na}$ inhibition. Accordingly, XE991 may not be an ideal compound to evaluate the influence of blocking $I_M$ on nerve excitability, at least in the mouse vagal sensory system.

Consistent with its inhibitory effect on AP generation in nodose C-fibers terminating in the lungs, retigabine effectively suppressed irritant gas–evoked coughing in awake mice. Mechanistically, how inhaled $SO_2$ and $NH_3$ activate airway sensory afferents and elicit coughs is unclear. The hydrophilic properties of $SO_2$ suggest it can readily dissolve in the lining fluid covering the mucosa of the respiratory tract and lower the pH, which in turn can activate TRPV1 and acid-sensing ion channels (55, 56). On the other hand, $NH_3$ can rapidly diffuse across plasma membrane, causing intracellular alkalization, which has been shown to activate TRPV1 and TRPA1 (55, 57). Activation of these ion channels is known to cause depolarization and activation of airway vagal afferents, thereby triggering a series of reflex responses, including coughs (19). Opening M-channels by retigabine may counteract these depolarizing forces (regardless of the types of ion channels involved) and make the sensory fibers much less excitable by hyperpolarizing the neurons toward $E_K$ and reducing input resistance, thereby preventing coughs from the irritant gas stimulation. Although retigabine inhalation inhibits both $SO_2$- and $NH_3$-evoked coughs, it appears to be less effective for the response to a high concentration of $NH_3$. It is tempting to speculate that this may be related to the intracellular alkalization caused by $NH_3$, since pH is known to modulate the gating of numbers of ion channels. It has been shown that intracellular alkalization reduced the KCNQ1/KCNE1-mediated slowly activating delayed rectifier K+ current (58). If the same happened to the M-channels in mouse airway vagal afferents, it may in part offset the effects retigabine. Moreover, in addition to activating TRPV1 and TRPA1 channels, an increase in the intracellular pH has been shown to enhance depolarizing N-type $Ca^{2+}$ current (59) and hyperpolarization-activated cation current (60), thus further favoring membrane depolarization.

*Therapeutic potential*. Increased vagal C-fiber activity can contribute to the reflex bronchospasm and secretions that compromise lung function in asthma and COPD. In addition, inappropriate vagal sensory nerve stimulation can lead to subacute, and in some cases chronic, coughing, as well as sensations of dyspnea that are ill matched to lung function (19). In particular, chronic cough, which affects about 10% of the population, has very limited treatment options (61). Our results showed that local activation of M-channels significantly inhibits the excitability of vagal C-fibers innervating mouse lungs and suppresses the cough response to inhaled irritant gases in freely moving mice. If these findings are also observed in humans, the M-channel would be a rational therapeutic target for inflammatory airway diseases. In support of this idea, a recent study has shown that gabapentin, a neuromodulator previously found to be effective for treatment of refractory chronic cough in patients (61), potently activates M-channels composed of KCNQ3, KCNQ5 homomers, or KCNQ2/3 heteromers (62). Moreover, airway smooth muscle cells also express functional KCNQ/$K_v$7 channels, and activating these channels by flupirtine or retigabine has been shown to attenuate the histamine-induced constriction of human airways (63) and relax muscarinic-evoked airway contraction in rodents (64, 65). Therefore, a topical (inhaled) formulation of an M-channel activator could be a unique strategy to both inhibit vagal C-fiber hyperactivity and dilate bronchi, with minimal unwanted central or peripheral side effects.

## Methods

*Mice.* Male C57BL/6J mice (6–14 weeks, from the Jackson Laboratory) were used in this study.

*Labeling and isolation of nodose neurons*. In some studies, bronchopulmonary afferent neurons were retrogradely labeled using DiI (1,1′-dioctadecyl-3,3,3′,3′-tetramethylindocarbocyanine perchlorate; DiC18(3); Molecular Probes/Invitrogen) instilled into the tracheal lumen of anesthetized mice 5–9 days before experiments. The distribution of dye in the lungs, but not in trachea or esophagus, was verified at the time the animals were sacrificed for cell isolation.

Mice were killed by $CO_2$ inhalation. Both sides of jugular/nodose ganglia were dissected and cleared of adhering connective tissues. The lower two-thirds of ganglia (primarily nodose) were cut out for subsequent enzymatic digestion at 37°C using type 1A collagenase (2 mg/ml) and dispase II (2 mg/ml). The isolated nodose neurons were plated onto poly-D-lysine/laminin–coated coverslips and kept at 37°C in L-15 medium containing 10% FBS for use within 8 hours for cell collection or within 24 hours for patch clamp recordings.

**Table 1. Single-cell RT-PCR primer sequences**

| Gene | Primer, sequence | Product length |
|---|---|---|
| *Kcnq2* | Forward (5′-3′), TGGTGCTGATTGCCTCCATT; reverse (5′-3′) CACGGTCTGCCTTTACTTGGT | 742 bp |
| *Kcnq3* | Forward (5′-3′), AGCACCGTCAGAAGCACTTT; reverse (5′-3′), AAGAGACCCAGCTTTTGGCT | 196 bp |
| *Kcnq4* | Forward (5′-3′), GAGAGCTGGCCCTCTTGTTT; reverse (5′-3′), GCGGATTCGGTCTTTGATGC | 194 bp |
| *Kcnq5* | Forward (5′-3′), GCTCTCGAGGCAGTCAAGATT; reverse (5′-3′), ACCGTGACCTTCCAGTCCTT | 171 bp |
| *P2rx2* | Forward (5′-3′), GGGGCAGTGTAGTCAGCATC; reverse (5′-3′), TCAGAAGTCCCATCCTCCA | 241 bp |
| *Trpv1* | Forward (5′-3′), TCACCGTCAGCTCTGTTGTC; reverse (5′-3′), GGGTCTTTGAACTCGCTGTC | 285 bp |

*Single-cell RT-PCR assay*. Single unlabeled or retrogradely labeled nodose neurons identified under a fluorescence microscope were collected into a PCR tube (1 cell per tube) containing 1 μl RNAse inhibitor (RNaseOUT, Thermo Fisher Scientific; 2 U/μl) 2 hours after isolation and immediately snap-frozen. A sample of the bath solution from the vicinity of a neuron was collected from each coverslip for no-template experiments (bath control).

First-strand cDNA was synthesized using the SuperScript III First-Strand Synthesis System for RT-PCR (catalog 18080, Invitrogen) according to the manufacturer's recommendations. 1.2 μl of synthesized cDNA (or RNA control and bath control) was used for PCR amplification (50 cycles) for mouse *Trpv1*, *P2rx2*, and *Kcnq2–5* using custom-synthesized primers (Sigma-Aldrich) (Table 1) and the HotStar Taq Polymerase Kit (QIAGEN) in a final volume of 20 μl. PCR products were visualized in ethidium bromide–stained 1.5% agarose gels.

The Kcnq genes were first screened in mouse nodose ganglia with cDNA synthesized from total RNA isolated from mouse brain, heart, and/or skeletal muscle as positive controls. *Kcnq1*, abundant in the heart, was not detected in nodose ganglia. Hence, only *Kcnq2–5* that were found in whole ganglia were examined in the single-neuron PCR assay.

*Patch clamp recording and analysis*. The amphotericin B/perforated whole-cell patch clamp technique was employed to record membrane potential and $I_M$ in nodose neurons at room temperature under current-clamp and voltage-clamp mode, respectively, using an Axopatch 200B amplifier interfaced with an Axon Digidata 1550A and driven by pCLAMP 10 software (Molecular Devices). Membrane currents were sampled at 5–10 kHz and filtered at 2–5 kHz. Bath solution contained (in mM) NaCl 136, KCl 5.4, $MgCl_2$ 1, $CaCl_2$ 1, HEPES 10, and glucose 10 (pH 7.35 with NaOH). To record $I_M$ with a holding potential of –30 mV, 1 mM CsCl was added to block HCN currents. Pipette solution contained (in mM) KCl 20, K-gluconate 125, and HEPES 10 (pH 7.2 with KOH). Freshly prepared amphotericin B was added to the pipette solution (300 μg/ml) before experiments. The junction potential (–14.7 mV estimated using Clampex calculator) was corrected.

Conventional whole-cell patch clamp technique was used to record $I_{Na}$. Bath solution contained (in mM): choline-Cl 126, NaCl 10, CsCl 3, TEA-Cl 5, $MgCl_2$ 1, $CaCl_2$ 1, $CdCl_2$ 0.1, HEPES 10, and glucose 10 (pH 7.35 with CsOH). Pipette solution contained (in mM): CsF 140, NaCl 10, $MgCl_2$ 1, $CaCl_2$ 0.1, EGTA 1.1, and HEPES 10 (pH 7.2 with CsOH). The current was sampled at 50 kHz and filtered at 10 kHz. The effect of XE991 on $I_{Na}$ was evaluated 8–10 minutes after the whole-cell formation when the current became relatively stable. For all voltage-clamp experiments, the cell capacitance and series resistance (80%) were compensated electronically.

Patch clamp recordings were analyzed using Clampfit 10. The steady-state activation of $I_M$ was assessed by measuring tail currents ($I_{tail}$) at –60 mV following long voltage steps to different potentials. The amplitude of $I_{tail}$ was measured at the peak after correcting for the leak current if necessary. To obtain the activation parameters, data points were fitted to the Boltzmann function for each cell: $I = G_{max}/(1 + \exp(-(V_m - V_{0.5})/k))$, or $I/I_{max} = G_{max}/(1 + \exp(-(V_m - V_{0.5})/k))$ for normalized activation curves, where $G_{max}$ is maximal conductance, $V_m$ membrane potential, $V_{0.5}$ voltage at which 50% of activation occurs, and $k$ slope factor. The input resistance was calculated by dividing the voltage step (from –70 to –60 mV) by sustained current measured at the end of voltage pulse. The rheobase was measured as the lowest amount of depolarizing current (100 ms) needed to evoke a single AP. The AP threshold was measured by differentiating the AP voltage with respect to time ($dV/dt$) and defined as the voltage at which the deflection for $dV/dt$ is greater than zero. The AP amplitude was measure as the difference between the peak of upstroke and the resting potential. The peak of the rate of AP upstroke was measured as the positive peak of $dV/dt$.

*Isolated perfused nerve-lung preparation and extracellular recording*. Mice were killed by $CO_2$ inhalation and exsanguination. The blood from the pulmonary circulation was flushed out by injecting through the right heart 10 ml Krebs bicarbonate buffer (KBS) composed of (in mM) NaCl 118, KCl 5.7, $NaH_2PO_4$ 1.0, $MgSO_4$ 1.2, $CaCl_2$ 1.9, $NaHCO_3$ 25.0, dextrose 11.1, and gassed with 95 % $O_2$/5 % $CO_2$, pH 7.4. The airways and lungs with intact right-side extrinsic vagal innervations (including right jugular-nodose ganglia complex [JNC]) were dissected, and the tissue was pinned in a small Sylgard-lined Perspex chamber. The right JNC along with the rostral-most vagi were pulled through a small hole into an adjacent chamber for extracellular recording. The hole was then sealed with Vaseline so that the recording chamber and lungs were perfused separately (see Figure 6A). A piece of PE60 tubing was inserted into the trachea and connected to the infusion pump for continuous perfusion with KBS (35–37°C, 2 ml/min) of the lungs. Short cuts (<1-mm deep, 6–10 per lobe) were made on the lung surface to allow exit of the perfusate.

Extracellular recordings of single-unit activities were performed in nodose ganglion (lower two-thirds of JNC) using an aluminosilicate glass microelectrode filled with 3 M sodium chloride (electrode resistance ~2 MΩ). The signal was amplified (Microelectrode AC amplifier 1800, A-M Systems), filtered (low cutoff, 0.3 kHz; high cutoff, 1 kHz), and the recording was stored on a hard drive for offline analyses using the software NerveOfIt (sampling frequency 33 kHz, PHOCIS). The receptive field was identified using a concentric stimulation electrode (100 V, 0.5 ms, 1 Hz) sequentially positioned at different places on the surface of the lung lobes. When the evoked APs were recorded, the tissue was probed with a mechanical probe (von Frey hair, 60–1800 mN). The mechanosensitive receptive field was identified when the mechanical stimulus evoked a burst of APs. Conduction velocity was calculated by dividing the distance along the nerve pathway by the time between the stimulus artifact and the AP evoked by electrical stimulation of the mechanosensitive receptive field. In this study, only the fibers conducting in the C-fiber range (<1 m/s) were used.

α,β-MeATP was administered to the lung by adding a 1-ml bolus of KBS containing the appropriate concentration of the agonist to the tracheal perfusion. When the effects of XE991 or retigabine on agonist-induced AP discharge were examined, the KBS containing the drugs was given through tracheal perfusion for 30 minutes before the second bolus of agonist was applied.

*Cough measurements in awake mice*. The irritant gas–induced cough in awake free-moving mice was measured as previously described (66). Briefly, mice moved freely in a Plexiglas recording chamber (volume 160 ml). Room air was drawn through the chamber at a constant flow rate (300 ml/min). The $CO_2$ concentration and temperature of the outlet air were continuously monitored (~0.6% and ~24°C, respectively, at steady state). To identify cough reliably in moving mice with inherently unstable breathing, a telemetry sensor (Data Sciences International, model PA-C10) was surgically implanted in the intrapleural space to measure intrapleural pressure ($P_{ip}$) directly; in addition the pressure of the chamber ($P_{cham}$) was continuously recorded with a pressure transducer (Biopac, model TSD160A). Audio and video signals of the mouse movements were also recorded. Prior to experiments, the mouse was placed in the recording chamber for >30 minutes for adaptation. During the inhalation challenge, a gas mixture of $SO_2$ or $NH_3$ was drawn into the chamber (replacing room air) at the same flow rate (300 ml/min) for 5 minutes. All signals were recorded before, during and after each inhalation challenge, each for a 5-minute duration.

The reason cough was determined not only by the recording chamber pressure (change in respiratory flow) and the intrathoracic pressure, but also by simultaneous audio-video recording of the animal's motion and action, was that it allowed us to identify coughs and also to distinguish them from sneezes, sniffs, and other respiratory actions. We did observe sneezes triggered occasionally in the early response to inhaled irritant gases such as $SO_2$ in awake mice, though they disappeared completely during the recovery from exposure to $SO_2$. Furthermore, sneezes typically did not generate peak intrathoracic pressure (recorded by telemetry sensor) greater than 40 mmHg; and the sound generated by sneeze was not as distinct as that by cough. As such, sneezes were not included in our data analysis of cough response.

Two concentrations of $SO_2$ (300 and 600 ppm) and $NH_3$ (0.1% and 0.2%) balanced in air were tested in each animal. At least 30 minutes was allowed for a full recovery between 2 consecutive challenges. The control (without retigabine) experiments were repeated 3 times on 3 separate days in each mouse. The effect of retigabine on cough sensitivity was tested at least 24 hours after completion of control experiments and repeated once 1–2 days later to test reproducibility. Retigabine aerosol (250 μM) was generated by a ultrasonic nebulizer (Lumiscope 6610) and administered to the mouse in an exposure chamber for 15 minutes. Five minutes later, the inhalation challenges were carried out. The sequence of $SO_2$ and $NH_3$ as well as the high/low concentrations of each gas was alternated between days in each mouse to achieve a balanced design.

*Statistics*. All statistical analyses were performed using SigmaPlot software (Systat). Pooled data are expressed as mean ± SEM. The statistical significance of differences between 2 means was determined by using either paired or unpaired Student's *t* test, as appropriate. In the cases in which the normality test failed, Wilcoxon's signed-rank test or Mann-Whitney rank-sum test was used as appropriate. The significance of differences between multiple means was evaluated by 1-way repeated-measures ANOVA. The significance of differences between 2 or multiple means and with different levels of treatment was evaluated by 2-way repeated-measures ANOVA. Holm-Šídák or Fisher's test as a post hoc analysis was performed for multiple pairwise comparisons. A *P* value less than 0.05 was considered significant.

*Study approval*. All experiments carried out were approved by IACUC of Johns Hopkins University and University of Kentucky.

## Author contributions

HS designed research studies, conducted experiments, analyzed data, and wrote the manuscript; AHL, FR, MJP, and SM conducted experiments and analyzed data; LYL designed research studies and analyzed data; BJU designed research studies and wrote the manuscript.

## Acknowledgments

This study was supported by Johns Hopkins Blaustein Pain Research Fund Grant and NIH grants R01 HL122228 and U01 AI123832.

Address correspondence to: Bradley J. Undem, 5501 Hopkins Bayview Circle, JHAAC 3A.44, Baltimore, Maryland 20224, USA. Phone: 410.550.2160; Email: bundem@jhmi.edu.

1. Lehman A, et al. Loss-of-function and gain-of-function mutations in KCNQ5 Cause intellectual disability or epileptic encephalopathy. *Am J Hum Genet*. 2017;101(1):65–74.
2. Maljevic S, Wuttke TV, Seebohm G, Lerche H. KV7 channelopathies. *Pflugers Arch*. 2010;460(2):277–288.
3. Brown DA, Adams PR. Muscarinic suppression of a novel voltage-sensitive K+ current in a vertebrate neurone. *Nature*. 1980;283(5748):673–676.
4. Brown BS, Yu SP. Modulation and genetic identification of the M channel. *Prog Biophys Mol Biol*. 2000;73(2-4):135–166.
5. Brown DA, Passmore GM. Neural KCNQ (Kv7) channels. *Br J Pharmacol*. 2009;156(8):1185–1195.
6. Schroeder BC, Kubisch C, Stein V, Jentsch TJ. Moderate loss of function of cyclic-AMP-modulated KCNQ2/KCNQ3 K+ channels causes epilepsy. *Nature*. 1998;396(6712):687–690.
7. Biervert C, et al. A potassium channel mutation in neonatal human epilepsy. *Science*. 1998;279(5349):403–406.
8. Charlier C, et al. A pore mutation in a novel KQT-like potassium channel gene in an idiopathic epilepsy family. *Nat Genet*. 1998;18(1):53–55.
9. Hansen HH, Waroux O, Seutin V, Jentsch TJ, Aznar S, Mikkelsen JD. Kv7 channels: interaction with dopaminergic and serotonergic neurotransmission in the CNS. *J Physiol (Lond)*. 2008;586(7):1823–1832.
10. Gunthorpe MJ, Large CH, Sankar R. The mechanism of action of retigabine (ezogabine), a first-in-class K+ channel opener for the treatment of epilepsy. *Epilepsia*. 2012;53(3):412–424.
11. Large CH, et al. The spectrum of anticonvulsant efficacy of retigabine (ezogabine) in animal models: implications for clinical use. *Epilepsia*. 2012;53(3):425–436.
12. Rivera-Arconada I, Roza C, Lopez-Garcia JA. Enhancing m currents: a way out for neuropathic pain? *Front Mol Neurosci*. 2009;2:10.
13. Du X, Gao H, Jaffe D, Zhang H, Gamper N. M-type K+ channels in peripheral nociceptive pathways. *Br J Pharmacol*. 2018;175(12):2158–2172.
14. Linley JE, Rose K, Ooi L, Gamper N. Understanding inflammatory pain: ion channels contributing to acute and chronic nociception. *Pflugers Arch*. 2010;459(5):657–669.
15. Wu Z, et al. Activation of KCNQ channels suppresses spontaneous activity in dorsal root ganglion neurons and reduces chronic pain after spinal cord injury. *J Neurotrauma*. 2017;34(6):1260–1270.
16. Wladyka CL, Feng B, Glazebrook PA, Schild JH, Kunze DL. The KCNQ/M-current modulates arterial baroreceptor function at the sensory terminal in rats. *J Physiol (Lond)*. 2008;586(3):795–802.
17. Peiris M, Hockley JR, Reed DE, Smith ESJ, Bulmer DC, Blackshaw LA. Peripheral KV7 channels regulate visceral sensory function in mouse and human colon. *Mol Pain*. 2017;13:1744806917709371.
18. Hirano K, Kuratani K, Fujiyoshi M, Tashiro N, Hayashi E, Kinoshita M. Kv7.2-7.5 voltage-gated potassium channel (KCNQ2-5) opener, retigabine, reduces capsaicin-induced visceral pain in mice. *Neurosci Lett*. 2007;413(2):159–162.
19. Mazzone SB, Undem BJ. Vagal afferent innervation of the airways in health and disease. *Physiol Rev*. 2016;96(3):975–1024.
20. Nassenstein C, et al. Phenotypic distinctions between neural crest and placodal derived vagal C-fibres in mouse lungs. *J Physiol (Lond)*. 2010;588(Pt 23):4769–4783.
21. Wladyka CL, Kunze DL. KCNQ/M-currents contribute to the resting membrane potential in rat visceral sensory neurons. *J Physiol (Lond)*. 2006;575(pt 1):175–189.
22. Greene DL, Kang S, Hoshi N. XE991 and linopirdine are state-dependent inhibitors for Kv7/KCNQ channels that favor activated single subunits. *J Pharmacol Exp Ther*. 2017;362(1):177–185.

23. Robbins J. KCNQ potassium channels: physiology, pathophysiology, and pharmacology. *Pharmacol Ther*. 2001;90(1):1–19.
24. Kwong K, Kollarik M, Nassenstein C, Ru F, Undem BJ. P2X2 receptors differentiate placodal vs. neural crest C-fiber phenotypes innervating guinea pig lungs and esophagus. *Am J Physiol Lung Cell Mol Physiol*. 2008;295(5):L858–L865.
25. Wang J, et al. Distinct and common expression of receptors for inflammatory mediators in vagal nodose versus jugular capsaicin-sensitive/TRPV1-positive neurons detected by low input RNA sequencing. *PLoS ONE*. 2017;12(10):e0185985.
26. Kollarik M, et al. Different role of TTX-sensitive voltage-gated sodium channel (NaV 1) subtypes in action potential initiation and conduction in vagal airway nociceptors. *J Physiol (Lond)*. 2018;596(8):1419–1432.
27. Lerche C, et al. Molecular cloning and functional expression of KCNQ5, a potassium channel subunit that may contribute to neuronal M-current diversity. *J Biol Chem*. 2000;275(29):22395–22400.
28. Schroeder BC, Hechenberger M, Weinreich F, Kubisch C, Jentsch TJ. KCNQ5, a novel potassium channel broadly expressed in brain, mediates M-type currents. *J Biol Chem*. 2000;275(31):24089–24095.
29. Selyanko AA, Hadley JK, Wood IC, Abogadie FC, Jentsch TJ, Brown DA. Inhibition of KCNQ1-4 potassium channels expressed in mammalian cells via M1 muscarinic acetylcholine receptors. *J Physiol (Lond)*. 2000;522(pt 3):349–355.
30. Kubisch C, et al. KCNQ4, a novel potassium channel expressed in sensory outer hair cells, is mutated in dominant deafness. *Cell*. 1999;96(3):437–446.
31. Yang WP, et al. Functional expression of two KvLQT1-related potassium channels responsible for an inherited idiopathic epilepsy. *J Biol Chem*. 1998;273(31):19419–19423.
32. Selyanko AA, Hadley JK, Brown DA. Properties of single M-type KCNQ2/KCNQ3 potassium channels expressed in mammalian cells. *J Physiol (Lond)*. 2001;534(Pt 1):15–24.
33. Tatulian L, Delmas P, Abogadie FC, Brown DA. Activation of expressed KCNQ potassium currents and native neuronal M-type potassium currents by the anti-convulsant drug retigabine. *J Neurosci*. 2001;21(15):5535–5545.
34. Roche JP, Westenbroek R, Sorom AJ, Hille B, Mackie K, Shapiro MS. Antibodies and a cysteine-modifying reagent show correspondence of M current in neurons to KCNQ2 and KCNQ3 K+ channels. *Br J Pharmacol*. 2002;137(8):1173–1186.
35. Li Y, Gamper N, Shapiro MS. Single-channel analysis of KCNQ K+ channels reveals the mechanism of augmentation by a cysteine-modifying reagent. *J Neurosci*. 2004;24(22):5079–5090.
36. Wickenden AD, Zou A, Wagoner PK, Jegla T. Characterization of KCNQ5/Q3 potassium channels expressed in mammalian cells. *Br J Pharmacol*. 2001;132(2):381–384.
37. Schwarz JR, et al. KCNQ channels mediate IKs, a slow K+ current regulating excitability in the rat node of Ranvier. *J Physiol (Lond)*. 2006;573(pt 1):17–34.
38. Battefeld A, Tran BT, Gavrilis J, Cooper EC, Kole MH. Heteromeric Kv7.2/7.3 channels differentially regulate action potential initiation and conduction in neocortical myelinated axons. *J Neurosci*. 2014;34(10):3719–3732.
39. King CH, Lancaster E, Salomon D, Peles E, Scherer SS. Kv7.2 regulates the function of peripheral sensory neurons. *J Comp Neurol*. 2014;522(14):3262–3280.
40. Pan Z, et al. A common ankyrin-G-based mechanism retains KCNQ and NaV channels at electrically active domains of the axon. *J Neurosci*. 2006;26(10):2599–2613.
41. Wang HS, et al. KCNQ2 and KCNQ3 potassium channel subunits: molecular correlates of the M-channel. *Science*. 1998;282(5395):1890–1893.
42. Wickenden AD, Yu W, Zou A, Jegla T, Wagoner PK. Retigabine, a novel anti-convulsant, enhances activation of KCNQ2/Q3 potassium channels. *Mol Pharmacol*. 2000;58(3):591–600.
43. Main MJ, Cryan JE, Dupere JR, Cox B, Clare JJ, Burbidge SA. Modulation of KCNQ2/3 potassium channels by the novel anticonvulsant retigabine. *Mol Pharmacol*. 2000;58(2):253–262.
44. Hadley JK, Noda M, Selyanko AA, Wood IC, Abogadie FC, Brown DA. Differential tetraethylammonium sensitivity of KCNQ1-4 potassium channels. *Br J Pharmacol*. 2000;129(3):413–415.
45. Shapiro MS, Roche JP, Kaftan EJ, Cruzblanca H, Mackie K, Hille B. Reconstitution of muscarinic modulation of the KCNQ2/KCNQ3 K(+) channels that underlie the neuronal M current. *J Neurosci*. 2000;20(5):1710–1721.
46. Schwake M, Pusch M, Kharkovets T, Jentsch TJ. Surface expression and single channel properties of KCNQ2/KCNQ3, M-type K+ channels involved in epilepsy. *J Biol Chem*. 2000;275(18):13343–13348.
47. Chung HJ, Jan YN, Jan LY. Polarized axonal surface expression of neuronal KCNQ channels is mediated by multiple signals in the KCNQ2 and KCNQ3 C-terminal domains. *Proc Natl Acad Sci USA*. 2006;103(23):8870–8875.
48. Rasmussen HB, et al. Requirement of subunit co-assembly and ankyrin-G for M-channel localization at the axon initial segment. *J Cell Sci*. 2007;120(Pt 6):953–963.
49. Heidenreich M, et al. KCNQ4 K(+) channels tune mechanoreceptors for normal touch sensation in mouse and man. *Nat Neurosci*. 2011;15(1):138–145.
50. Schütze S, Orozco IJ, Jentsch TJ. KCNQ potassium channels modulate sensitivity of skin down-hair (D-hair) mechanoreceptors. *J Biol Chem*. 2016;291(11):5566–5575.
51. Barkai O, Goldstein RH, Caspi Y, Katz B, Lev S, Binshtok AM. The Role of Kv7/M potassium channels in controlling ectopic firing in nociceptors. *Front Mol Neurosci*. 2017;10:181.
52. Romero M, Reboreda A, Sánchez E, Lamas JA. Newly developed blockers of the M-current do not reduce spike frequency adaptation in cultured mouse sympathetic neurons. *Eur J Neurosci*. 2004;19(10):2693–2702.
53. Vetter I, et al. Amplified cold transduction in native nociceptors by M-channel inhibition. *J Neurosci*. 2013;33(42):16627–16641.
54. Passmore GM, et al. Functional significance of M-type potassium channels in nociceptive cutaneous sensory endings. *Front Mol Neurosci*. 2012;5:63.
55. Dhaka A, et al. TRPV1 is activated by both acidic and basic pH. *J Neurosci*. 2009;29(1):153–158.
56. Canning BJ. Afferent nerves regulating the cough reflex: mechanisms and mediators of cough in disease. *Otolaryngol Clin North Am*. 2010;43(1):15–vii.
57. Fujita F, et al. Intracellular alkalization causes pain sensation through activation of TRPA1 in mice. *J Clin Invest*. 2008;118(12):4049–4057.
58. Unsöld B, et al. KCNE1 reverses the response of the human K+ channel KCNQ1 to cytosolic pH changes and alters its pharma-

cology and sensitivity to temperature. *Pflugers Arch*. 2000;441(2-3):368–378.
59. Kiss L, Korn SJ. Modulation of N-type Ca2+ channels by intracellular pH in chick sensory neurons. *J Neurophysiol*. 1999;81(4):1839–1847.
60. Munsch T, Pape HC. Modulation of the hyperpolarization-activated cation current of rat thalamic relay neurones by intracellular pH. *J Physiol (Lond)*. 1999;519 Pt 2:493–504.
61. Ryan NM, Birring SS, Gibson PG. Gabapentin for refractory chronic cough: a randomised, double-blind, placebo-controlled trial. *Lancet*. 2012;380(9853):1583–1589.
62. Manville RW, Abbott GW. Gabapentin is a potent activator of KCNQ3 and KCNQ5 potassium channels. *Mol Pharmacol*. 2018;94(4):1155–1163.
63. Brueggemann LI, et al. Kv7 potassium channels in airway smooth muscle cells: signal transduction intermediates and pharmacological targets for bronchodilator therapy. *Am J Physiol Lung Cell Mol Physiol*. 2012;302(1):L120–L132.
64. Evseev AI, et al. Functional effects of KCNQ K(+) channels in airway smooth muscle. *Front Physiol*. 2013;4:277.
65. Brueggemann LI, et al. KCNQ (Kv7) potassium channel activators as bronchodilators: combination with a β2-adrenergic agonist enhances relaxation of rat airways. *Am J Physiol Lung Cell Mol Physiol*. 2014;306(6):L476–L486.
66. Zhang C, Lin RL, Hong J, Khosravi M, Lee LY. Cough and expiration reflexes elicited by inhaled irritant gases are intensified in ovalbumin-sensitized mice. *Am J Physiol Regul Integr Comp Physiol*. 2017;312(5):R718–R726.